Tellus (1978), *30*, 323–334

Growth rate and vertical propagation of the initial error in baroclinic models

By LENNART BENGTSSON, *European Centre for Medium Range Weather Forecasts Fitzwilliam House, Skimped Hill, Bracknell, Berkshire RG12 1LQ, England*

(Manuscript received May 16; in final form December 19, 1977)

ABSTRACT

The present study investigates the growth of error in baroclinic waves. It is found that stable or neutral waves are particularly sensitive to errors in the initial condition. Short stable waves are mainly sensitive to phase errors and the ultra long waves to amplitude errors. Analysis simulation experiments have indicated that the amplitudes of the very long waves become usually too small in the free atmosphere, due to the sparse and very irregular distribution of upper air observations. This also applies to the four-dimensional data assimilation experiments, since the amplitudes of the very long waves are usually underpredicted. The numerical experiments reported here show that if the very long waves have these kinds of amplitude errors in the upper troposphere or lower stratosphere the error is rapidly propagated (within a day or two) to the surface and to the lower troposphere.

1. Introduction

Errors in numerical weather prediction are due to many different causes. There are errors in the initial state caused by errors in the observations and errors due to the scarcity of observations. There are numerical or mathematical errors caused by approximations of the prediction equations and errors due to an improper parameterization of the sub-grid scale processes. It is not possible to perform a stringent separation of these causes since they in fact are strongly interrelated. Robert (1974) has done a crude estimate of the sources of error in short range prediction. Giving the total error as 100% he estimated the fractions of errors as follows

(i) Observational errors 18%
(ii) Numerical errors 48%
(iii) Sub-grid scale processes 34%.

Robert's study was based on the error budget for North America (good data coverage), a 5-level model with 381-km grid at 60° N and second-order finite differences. It is evident that if a similar study was carried out for Europe and the North Atlantic region using a reference model of higher resolution, the numerical errors would be reduced and the observational errors increased. The errors in the initial state are perhaps the easiest to understand and diagnose. Given a certain observing network and knowing the statistical structure of the meteorological parameter and its observational error one can easily map the interpolation error (Gandin, 1960). Fig. 1 and Fig. 2 show the interpolation error for the 500-mb geopotential at the Northern Hemisphere and Southern Hemisphere respectively based upon the WMO network of radiosonde stations 1976 and calculated from climatology as a norm. Due to the systematic variations in station density between land and ocean areas, this will also cause large scale errors in the initial state. Bengtsson and Gustafsson (1972) calculated the initial error for a test case from December 1967 and stratified the initial error in four different zonal wave number components between 30°–60° N. It was found that the analysis error was relatively uniformly distributed over the whole spectrum and even the error in the ultra long waves was substantial (see Table 1). Table 1 also presents the mean analysis error as well as the error for a data sparse area over the North Pacific. The particular area is given in the referred article.

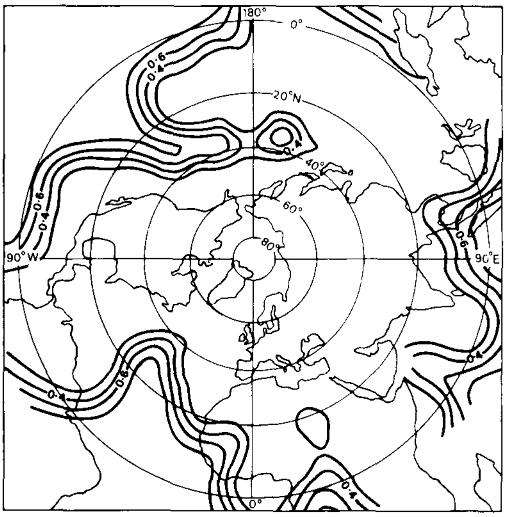

Fig. 1. The relative interpolation error normalized by the total variance for the geopotential at the Northern Hemisphere and based on the present (1976) WMO upper air network. Climatology is used as a norm. Isolines are drawn for every 20% increase of the relative interpolation. According to G. Larsen, ECMWF (personal communication).

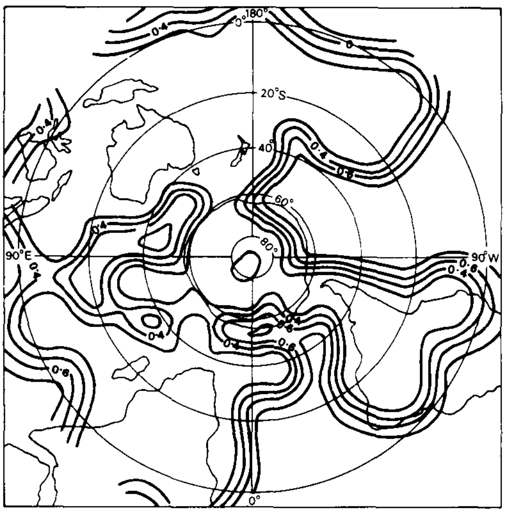

Fig. 2. The relative interpolation error nomalized by the total variance for the geopotential at the Southern Hemisphere and based on the present (1976) WMO upper air network. Climatology is used as a norm. Isolines are drawn for every 20% increase of the relative interpolation. According to G. Larsen, ECMWF (personal communication).

The application of a four-dimensional data assimilation will reduce this error and in Table 1 we can see how the error has been reduced after a 72-hour updating. Updating was done every 12 hours using the WMO upper air network. The analysis error levels off after about 72 hours and as can be seen from Table 1 the overall error is reduced by

Table 1. *Improvement of the initial RMS-error at 500 mb after 72 hours data assimilation. (Successive analysis and forecasting every 12 hours. WMO conventional network used.) Information compiled from Bengtsson and Gustafsson (1972)*

	RMS-errors 90° N–20° N	North Pacific
Initial error (climatology first guess)	45 m	115 m
After 72 hours updating (independent data set)	35 m (0.77)	60 m (0.52)
After 72 hours updating (ideal model assumption)	25 m (0.55)	35 m (0.30)

	RMS-errors in zonal wave components 30° N–60° N			
	1–3	4–6	7–9	10–20
Initial error	28 m	27 m	16 m	10 m
After 72 hours updating (ideal model assumption)	10 m	11 m	9 m	10 m

23% if we use an independent data set and 45% under ideal model assumption. Since the updating in this case was done with the equivalent barotropic model we may assume that using the most accurate prediction models of today we can reduce the overall error by about 35–40%. In data-sparse areas the improvement is much higher and the corresponding improvement over the data-sparse North Pacific is by 48% with an independent data set and by as much as 70% under ideal model assumptions. The error reduction in the zonal wave number components is of the same magnitude. A further reduction of the error can be expected if we introduce observations from satellites (temperatures from radiance measurements and wind from cloud picture elements) as well as from other conventional observations (SYNOP and AIREPS). However, recent simulation studies at ECMWF indicate that these improvements will be small at the Northern Hemisphere but substantial at the Southern Hemisphere.

A problem which has caused much concern is the rapid increase in the prediction error in the early phase of a numerical prediction. During the first 6–24 hours a rapid increase in the error is often observed. This error growth is noticed for all kinds of models, primitive as well as filtered, and has led to the fact that rather simple quasi-geostrophic models are often as good as sophisticated models based on the primitive equations for short range prediction. This is an indication that the error in the initial state in these situations is the dominating one. We will in this paper indicate a mechanism which can explain this rapid error growth. The result shows that the error growth is particularly large for stable or nearly stable baroclinic disturbances.

Another characteristic feature of the initial error is that the error generally increases with height. This is partly due to the fact that the observational network is best at the surface and then becomes successively worse the higher we come in the atmosphere and partly to an increased variance by height. We will show that under some circumstances and in particular for the very long waves we can have a very rapid propagation of the error in the vertical. This stresses the necessity of having an observing network and an analysis system which can give us homogeneous errors through the whole troposphere.

2. Methodology

In this investigation we will study the growth rate of the error in the initial state under some very simplified conditions. We will make use of the quasi-geostrophic equations and the β-plane approximation. We believe that the non-geostrophic processes do not play any significant role in studies of this kind and as has been shown by Moen (1974), baroclinic waves have the same basic characteristics for the quasi-geostrophic equations as for the complete primitive equations. We are going to study perturbations of finite amplitudes but we are not going to incorporate any interactions between the perturbation and the zonal flow. The zonal flow will be regarded as constant in time, nor will any other non-linear processes be included.

In the initial phase of an unstable baroclinic wave these approximations are not serious, since the induced zonal wind (Ferrel-circulation) as well as the cascade processes only become essential in the later stage when the wave is fully developed (Bengtsson, 1964). The stable baroclinic waves oscillate in time and have a small influence on the zonal flow unless the amplitude is very large.

There is a fundamental difference between an unstable and a stable wave in that sense that the final stage of an unstable wave is *independent* of the initial structure of the wave. The wave will under all circumstances grow and ultimately assume the structure of the unstable mode. In that sense the unstable wave is relatively independent of the initial conditions, since the wave in any case will assume a structure given by the initial wind field and the static stability (Ogura, 1957). Naturally, the closer the initial wave is to the final structure the sooner the wave will reach this stage. However, this is not the case for the stable baroclinic waves. These waves will always, as will be shown, depend strongly on the initial state and the amount of energy which will oscillate between kinetic and available potential energy as the wave propagates in time is given by the initial structure (variation of amplitude and phase with pressure) of the wave. It follows from this that the stable waves are extremely sensitive to the initial conditions. A natural question which arises is to what extent stable waves of finite amplitudes exist in the atmosphere and consequently to what degree the subsequent study is relevant. However, this is certainly not too uncommon in the atmosphere where cyclones are generated in areas of general instability and then move out into areas where the large scale conditions are unfavourable for a continued baroclinic growth of the wave or the cyclone. Such conditions are likely to occur downstream in areas of general cyclogenesis.

In order to arrive at a basic understanding of the sensitivity to the initial condition for a baroclinic wave, we shall start this investigation by analysing wave solutions of the most simple, non-trivial baroclinic systems. This is a system where the relation between wind and mass field is expressed by the linear part of the balance equations assuming a constant Coriolis parameter, f_0, and where the static stability only is allowed to vary in the vertical. The β-plane approximation is applied. Under these assumptions the model is governed by the vorticity equation and the thermal equation in the following form. In the p-system these equations read

$$\nabla^2 \frac{\partial \psi}{\partial t} + J(\psi, \nabla^2 \psi) + \beta \frac{\partial \psi}{\partial x} - f_0 \frac{\partial \omega}{\partial p} = 0 \qquad (2.1)$$

$$\frac{\partial^2 \psi}{\partial p \, \partial t} + J\left(\psi, \frac{\partial \psi}{\partial p}\right) + \frac{\sigma \omega}{f_0} = 0 \qquad (2.2)$$

where ψ is the stream function and $\sigma(p)$ the static stability.

It is possible to include some fundamental physical processes in a study of this kind. However, in this first attempt we will only include surface friction. The surface friction will be incorporated as the flux through a simple boundary layer. In such a case ω through the top of the boundary layer is proportional to the vorticity at the top of the boundary layer. Friction will, therefore, be incorporated as a lower boundary condition on ω and we will return to that below.

We will try to find a solution of (2.1) and (2.2) assuming solutions of the particular form:

$$\begin{aligned} \psi(x, y, p, t) &= -U(p)y + \psi(p, t)e^{i(kx+my)} \\ \omega(x, y, p, t) &= \Omega(p, t)e^{i(kx+my)} \end{aligned} \qquad (2.3)$$

Insertion of (2.3) in (2.1) and (2.2) gives

$$\frac{\partial \psi}{\partial t} = -Uik\psi + \frac{\beta ik}{k^2+m^2}\psi - \frac{f_0}{k^2+m^2}\frac{\partial \Omega}{\partial p} \qquad (2.4)$$

$$\frac{\partial^2 \psi}{\partial p \, \partial t} = ik\left(\psi \frac{dU}{dp} - U \frac{\partial \psi}{\partial p}\right) - \frac{\sigma \Omega}{f_0} \qquad (2.5)$$

Elimination of the time-derivative from eqs. (2.4) and (2.5) gives a diagnostic equation for Ω, the so-called ω-equation.

$$\frac{\partial^2 \Omega}{\partial p^2} - \frac{(k^2+m^2)\sigma}{f_0^2}\Omega = i\left\{\frac{\beta k}{f_0}\frac{\partial \psi}{\partial p} - \frac{2\psi k(k^2+m^2)}{f_0}\frac{dU}{dp}\right\} \qquad (2.6)$$

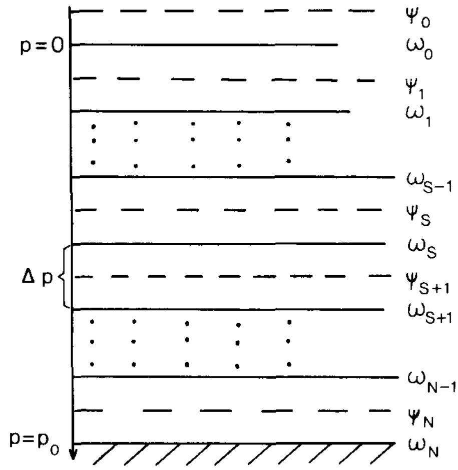

Fig. 3. The distribution of levels in the vertical. Vorticity equation is applied on dashed lines and ω-equation on full lines.

ψ and Ω are the unknowns and they are predicted by eqs. (2.4) and (2.6). They are functions of p and t. We will solve eqs. (2.4) and (2.6) by applying finite differences in the vertical (Fig. 3 gives the distribution of levels in the vertical). We then have

$$\left(\frac{\partial \psi}{\partial p}\right)_s = \frac{\psi_{s+1} - \psi_s}{\Delta p}$$

$$\left(\frac{\partial^2 \Omega}{\partial p^2}\right)_s = \frac{\Omega_{s+1} + \Omega_{s-1} - 2\Omega_s}{(\Delta p)^2}$$

$$\left(\frac{\partial \Omega}{\partial p}\right)_s = \frac{\Omega_s - \Omega_{s-1}}{\Delta p}$$

Insertion of these finite differences gives

$$\left(\frac{\partial \psi}{\partial t}\right)_s = ik\left(\frac{\beta}{k^2+m^2} - U_s\right)\psi_s - \frac{f_0}{(k^2\, m^2)\,\Delta p}(\Omega_s - \Omega_{s-1}) \qquad (2.7)$$

$$\Omega_{s+1} + \Omega_{s-1} - \left(2 + \frac{(\Delta p)^2(k^2+m^2)}{f_0^2}\sigma_s\right)\Omega_s = ik\left(\frac{\beta}{f_0}(\psi_{s+1} - \psi_s) - (\psi_{s+1} + \psi_s) \times (U_{s+1} - U_s)\frac{(k^2+m^2)}{f_0}\right) \qquad (2.8)$$

The 2-layer model (Section 3) is solved analytically while the 10-layer model in Section 4 is solved numerically. The numerical solution is performed in two steps. First eq. (2.8) is solved for $s = (1, N-1)$ by a direct method (see Appendix). The following boundary conditions are used

No friction	*Surface friction*
$\Omega_0 = 0$	$\Omega_0 = 0$
$\Omega_N = 0$	$\Omega_N = F_N(k^2 + m^2)\psi_N$

where F_N is a friction coefficient. $F_N = 1$ is a realistic value corresponding to a cross-isobaric flow of 10° and a surface wind speed 70% of the geostrophic wind.

3. Solutions for the 2-layer model

For a small vertical resolution eqs. (2.7) and (2.8) can with a reasonable amount of algebraic exercises be solved analytically. In order to have a general discussion on the properties of the different solutions and also to be able to check the numerical computations, we will solve the simple system where $N = 2$ and in the case of no friction. For further details see Ogure (1957).

Inserting (2.8) into (2.7) gives two ordinary differential equations in ψ_1 and ψ_2 viz

$$\begin{aligned} \dot{\psi}_1 &= k_1\psi_1 + k_2\psi_2 \\ \dot{\psi}_2 &= k_3\psi_2 + k_4\psi_1 \end{aligned} \tag{3.1}$$

where

$$\begin{aligned} k_1 &= -ik\frac{(\gamma + 1)(U_1 - C_B) + U_2}{\gamma + 2} \\ k_2 &= ik\frac{V + C_B}{\gamma + 2} \\ k_3 &= -ik\frac{(\gamma + 1)(U_2 - C_B) + U_1}{\gamma + 2} \\ k_4 &= -ik\frac{V - C_B}{\gamma + 2} \end{aligned} \tag{3.2}$$

Here

$\gamma = \dfrac{(\Delta p)^2(k^2 + m^2)}{f_0^2}\sigma_1$ represents the static stability times wave number square

$C_B = \dfrac{\beta}{k^2 + m^2}$ represents the phase speed due to the β-term

$V = U_2 - U_1$ represents the vertical wind shear.

The general solution to eq. (3.1) reads:

$$\begin{aligned} \psi_1(t) &= Ae^{\omega_1 t} + Be^{\omega_2 t} \\ \psi_2(t) &= Ce^{\omega_1 t} + De^{\omega_2 t} \end{aligned} \tag{3.3}$$

where A, B, C, D are complex coefficients and ω_1 and ω_2 are the roots to the characteristic equation of (3.1).

$$\omega_1, \omega_2 = \frac{k_1 + k_3}{2} \pm \sqrt{\left(\frac{k_1 + k_3}{2}\right)^2 - (k_1k_3 - k_2k_4)} \tag{3.4}$$

Inserting the initial condition $\psi_1 = \psi_1(0)$ and $\psi_2 = \psi_2(0)$ at $t = 0$ in 3.3 yields

$$\begin{aligned} \psi_1(t) = {} & \frac{e^{\omega_1 t}}{2D}\{\psi_1(0)(V\gamma + D) - 2\psi_2(0)(V + C_B)\} \\ & + \frac{e^{\omega_2 t}}{2D}\{\psi_1(0)(D - V\gamma) + 2\psi_2(0)(V + C_B)\} \end{aligned} \tag{3.5}$$

$$\begin{aligned} \psi_2(t) = {} & \frac{e^{\omega_1 t}}{2D}\{\psi_2(0)(D - V\gamma) - 2\psi_1(0)(V + C_B)\} \\ & + \frac{e^{\omega_2 t}}{2D}\{\psi_2(0)(D + V\gamma) + 2\psi_1(0)(V + C_B)\} \end{aligned} \tag{3.6}$$

where $D = \sqrt{(V)^2(\gamma^2 - 4) + 4C_B^2}$

In the following we will restrict the discussion to the behaviours of stable waves where

$$(V)^2(\gamma^2 - 4) + 4C_B^2 > 0 \tag{3.7}$$

We will next separate $\psi(t)$ into a part representing amplitude and one part representing phase. If $\alpha(t)$ represent amplitude and $\delta(t)$ phase we get the relation

$$\psi(t) = \alpha(t)e^{i\delta(t)} \tag{3.8}$$

Inserting (3.8) into (3.5) and (3.6) we can derive the following expression for the change of amplitude in time at the two levels:

$$\begin{aligned} \alpha_1^2(t) = {} & \alpha_1^2(0)\cos^2\omega t + D^{-2}\sin^2\omega t\{\alpha_1^2(0)V^2\gamma^2 \\ & + 4\alpha_2^2(0)(C_B + V)^2 - 4\alpha_1(0)\alpha_2(0)V\gamma(C_B + V) \\ & \times \cos(\delta_2(0) - \delta_1(0))\} - 2\alpha_1(0)\alpha_2(0) \\ & \times D^{-1}(C_B + V)\sin 2\omega t \sin(\delta_2(0) - \delta_1(0)) \end{aligned} \tag{3.9}$$

$$\alpha_2^2(t) = \alpha_2^2(0)\cos^2\omega t + D^{-2}\sin^2\omega t\{\alpha_2^2(0)V^2\gamma^2 + 4\alpha_1^2(0)(C_B - V)^2 - 4\alpha_2(0)\alpha_1(0)\,V\gamma(V - C_B) \times \cos(\delta_2(0) - \delta_1(0))\} - 2\alpha_2(0)\alpha_1(0) \times D^{-1}(V - C_B)\sin 2\,\omega t \sin(\delta_2(0) - \delta_1(0)) \tag{3.10}$$

here

$$\omega = \tfrac{1}{2}(\omega_2 - \omega_1) = \frac{kD}{2(2+\gamma)} \tag{3.11}$$

As can be seen from the eqs. (3.9) and (3.10) the stable waves oscillate in amplitude as the wave moves along. The phase of the stable wave oscillates as well. When the phase tilts in a direction opposite the direction in which the wave moves the wave will grow and when the phase tilts the other direction the amplitude of the wave will decrease. The unstable waves on the other hand have a different solution which is obtained by replacing sin and cos with sinh and cosh respectively. This wave grows, independently of its initial structure, and assumes finally the structure of the unstable mode. The unstable mode has a given constant phase-lag which is such that the continuous growth of the wave is favoured.

In the 2-layer model there are two stable regimes, one for short waves and another one for long waves according to relation (3.7). Let us first study the properties of eq. (3.10) for short stable waves.

3.1. Short stable waves

In order to simplify the investigation, we will make the approximation $V \gg C_B$ that is the phase speed of the short waves is not reduced very much by the β-effect. This implies unless γ is very close to 2 that $D \sim V(\gamma^2 - 4)^{1/2}$. Equation (3.10) then gets the following approximative form

$$\alpha_2^2(t) = \cos^2\omega t + \sin^2\omega t\left\{\frac{\gamma^2 + 4 - 4\gamma\cos(\delta_2 - \delta_1)}{\gamma^2 - 4}\right\} - \sin 2\omega t\,\{2(\gamma^2 - 4)^{-1/2}\sin(\delta_2 - \delta_1)\} \tag{3.12}$$

We will first investigate eq. (3.12) with respect to variation in the initial phase-lag, $\delta_2(0) - \delta_1(0)$. We will then let the initial amplitude be the same at both levels and we will further put $\alpha_1(0) = \alpha_2(0) = 1$. As is seen from eq. (3.12) and also from the complete eqs. (3.9) and (3.10) the solutions consist of an oscillating wave with the period 2ω. As also can be seen the magnitude of the oscillation for a given value of γ, depends critically on the initial phase-difference $\delta_2(0) - \delta_1(0)$ between the lower and higher level.

Let us take two extreme cases, namely, I when $\delta_2(0) - \delta_1(0) = 0$ respectively II $\delta_2(0) - \delta_1(0) = -\pi$

$\delta_2(0) - \delta_1(0) = 0$ implies

$$\text{I} \quad \alpha_2^2(t) = 1 - \frac{4}{\gamma + 2}\sin^2\omega t \quad \text{for } \gamma > 2$$

$$\delta_2(0) - \delta_1(0) = -\pi$$

$$\text{II} \quad \alpha_2^2(t) = 1 + \frac{4}{\gamma - 2}\sin^2\omega t \quad \text{for } \gamma > 2$$

In case I the initial amplitude will *decrease* from 1 to

$$\left(\frac{\gamma - 2}{\gamma + 2}\right)^{1/2} \text{ from } t = 0 \text{ to } t = \frac{\pi(2+\gamma)}{kD} \sim \frac{L}{V}\left(\frac{\gamma + 2}{\gamma - 2}\right)^{1/2}$$

and then oscillate between 1 and $\left(\frac{\gamma - 2}{\gamma + 2}\right)^{1/2}$

In case II the initial amplitude will *increase* from 1 to

$$\left(\frac{\gamma + 2}{\gamma - 2}\right)^{1/2} \text{ from } t = 0 \text{ to } t = \frac{\pi(2+\gamma)}{kD}$$

and then oscillate between 1 and $\left(\frac{\gamma + 2}{\gamma - 2}\right)^{1/2}$

Fig. 4 shows the difference between case I and case II as a function of γ. For stable waves the energy will *oscillate* between kinetic energy and available potential energy and the amount of this energy depends upon the initial structure (phase-lag) of the initial wave. For smaller variations in the phase-lag the variations are smaller but still substantial. Fig. 5 shows the result for a wave where $L = M = 4000$ km, $\sigma = 3$ (MTS-units) and $V = 30$ m s^{-1}. Integration has been carried out at 60°N for $\delta_2(0) - \delta_1(0) = -90°, -45°, 0°$ and $+45°$. In this case the computation has been carried out for the complete equation (3.10). As can be seen the amount of energy oscillating between available potential energy and kinetic energy varies considerably and depends critically on the initial phase-lag.

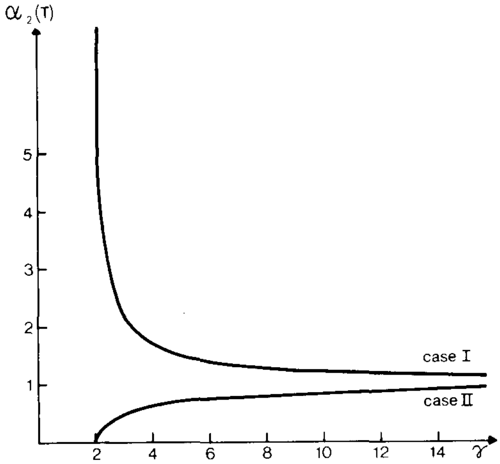

Fig. 4. Case I is the minimum value the amplitude of an oscillating stable wave will obtain after the time

$$T \sim \frac{L}{V}\left(\frac{\gamma+2}{\gamma-2}\right)^{1/2}$$

and case II the maximum value the amplitude of an oscillating stable wave will obtain after the time T.

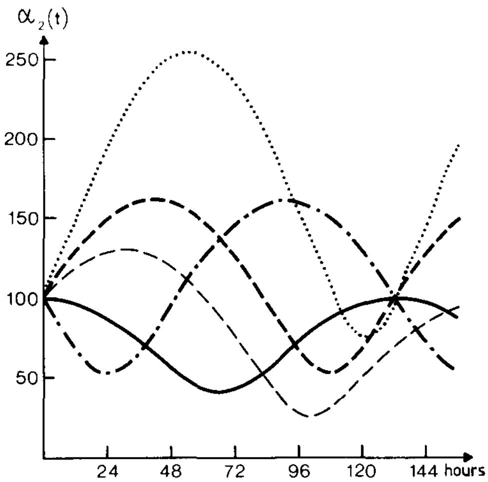

Fig. 5. The variation of amplitude at the lowest level of the 2-layer model in time for different values on the initial phase-lag. Full line shows the case with 0° phase-lag, dashed line −45° phase-lag, dash-dotted line +45° phase-lag and the dotted line presents the case with a −90° phase-lag. Thin dashed line shows the case with a −45° phase-lag with Ekman friction included.

We will next investigate how the change of the amplitude at the lower level $\alpha_2(t)$ is influenced by the size of the amplitude at the upper level. Let us denote $\alpha_1(0) = r\alpha_2(0)$. In this case we will keep $\delta_2(0) - \delta_1(0) = 0$, that is we will have no phase-lag initially. Applying the same assumption as above we get the relation for the amplitude at the lower level

$$\alpha_2^2(t) = 1 + \frac{4(r^2 + 1 - r\gamma)}{\gamma^2 - 4}\sin^2\omega t \tag{3.13}$$

Fig. 6 gives the amplitude at $t = \dfrac{L}{V}\left(\dfrac{\gamma+2}{\gamma-2}\right)^{1/2}$ for four different values of r and as a function of γ.

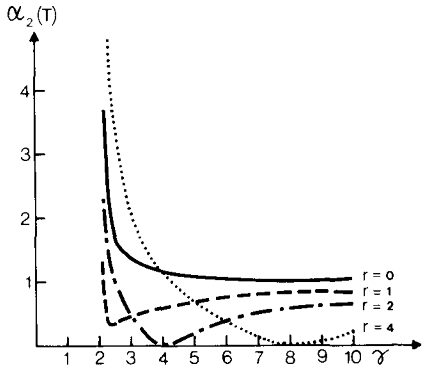

Fig. 6. The amplitude $\alpha_2\,(T)$ after the time

$$T = \frac{\pi(2+\gamma)}{kD}$$

when the amplitude reaches a maximum of a minimum value. The initial amplitudes are $\alpha_2(0) = 1$ and $\alpha_1(0) = r$. When $\gamma \to \infty$ $\alpha_2 \to 1$.

It is evident from the result presented in Figs. 2–4 that the short stable waves are very sensitive to the initial conditions. In particular the initial phase-lag of the wave is important to know with high accuracy if we want accurate prediction of the wave. This result is in agreement with our experience in short range numerical prediction. It has been demonstrated on several occasions that predictions of cyclone waves with short wavelengths of 2000–3000 km are very sensitive to the initial conditions. In the same way operational numerical forecasts of 24–36 hours either based on the filtered or the primitive equation often predict cyclone development satisfactory if they initially are found in areas with a satisfactory and homogeneous network and consequently have small errors through the whole depth of the atmosphere.

3.2. Ultra long waves

We will next turn our attention to the very long waves. In order to simplify the basic understanding we will try to reduce eq. (3.10) to a simpler form. For the very long waves $C_B > V$, in particular in cases where the vertical wind shear is relatively small. In the same way γ is of the order of 10^{-1} or less. If we after applying these assumptions only keep the dominating terms in eq. (3.10) we arrive at the following approximate form which we can apply for the very long waves

$$\alpha_2^2(t) = \alpha_2^2(0)\cos^2\omega t + \alpha_1^2(0)\sin^2\omega t + \alpha_1\alpha_2\sin(\delta_2 - \delta_1)\sin 2\omega t \tag{3.14}$$

ω is here the frequency of the wave which for the ultra long waves can be approximated

$$\omega \sim \frac{C_B \pi}{L}$$

If we in agreement with above put $\alpha_1(0) = r\alpha_2(0)$ and $\alpha_2(0) = 1$ we get

$$\alpha_2^2(t) = 1 + (r^2 - 1)\sin^2 \omega t + r\sin(\delta_2(0) - \delta_1(0))\sin 2\omega t \tag{3.15}$$

If we assume that $r = 0.8$ (assuming a 20% lower amplitude at the upper level) and put $C_B = 30$ m/s and $L = 10{,}000$ km we obtain an amplitude error (reduction) at the lower level of 20% after 48 hours. The initial phase-lag has been taken to be 0°.

It follows consequently from eq. (3.15) that also for the very long waves the prediction of the amplitudes is very sensitive to the error of the initial state. Making use of the same approximation as in the derivation of (3.15) we can compute a simplified expression for the phase-change of the very long waves. This expression reads:

$$\delta_2(t) = \operatorname{arctg}\{\sin\delta_2(0) + r\, tg\omega t\} \tag{3.16}$$

Here $\delta_2(0)$ is the initial phase at the lowest level and $\delta_2(t)$ is the phase at the same level at the time t. It has been assumed that $\delta_1(0) = 0$.

4. Solutions for a 10-layer model

We will now return to the complete system of eqs. (2.7) and (2.8). We will carry out a numerical integration of these equations using a vertical resolution of $N = 10$. (For details see Appendix.) This resolution can be regarded as satisfactory to describe quasi-geostrophic baroclinic waves on a β-plane (Hirota, 1968; Brown, 1969). The ω-equation (2.8) is solved by a direct method and the numerical solution of the vorticity equation is solved by a Runge-Kutta 4th order scheme. We have compared the numerical solution with the analytic solution for the 2-layer model and we have found the numerical method to be very accurate. The relative phase and amplitude error is of the order of 10^{-5}.

When the vertical resolution increases the band of unstable wavelengths increases. As was shown by Green (1960) all wavelengths became in fact unstable in the case of a continuous β-plane model. The problem has been discussed by Bretherton (1966) who connected the existence of short unstable waves with critical layer instability. This type of instability has a low growth rate and is limited vertically to a layer around a level where the real phase speed of the wave equals the zonal wind speed. The existence of a weak instability of this kind will lead to a somewhat more complicated behaviour of the waves than we have found for the simple 2-layer model and it is likely to expect an exponential growth of the amplitude superimposed on an oscillating mode. However, it is found that the oscillating mode dominates outside the regime of major instability. For the high resolution experiments we have used a zonal wind profile with a maximum around 250 mb and characteristic for middle latitudes during the winter. The wind profile as well as the specified static stability is given in Table 1. Fig. 7 gives the result for the amplitude at the lowest level for a short wave, $L = M = 2000$ km, very close to the stable cut off.

We have carried out the integrations for three different initial states characterized by rather small differences in the phase-lag. The initial amplitude is the same at all levels. The initial phase-lag as well as the zonal wind and the static stability is given in Table 2. The amplitude of this particular wave, which is slightly unstable, has pronounced maximum in the lower part of the atmosphere. The amplitude at 950 mb which is the lowest level is about six times as large as the amplitude around 500 mb. As can be seen from Fig. 7 the very small variations in the phase-lag of the wave, which are smaller than ± 250 km, give rise to deviations which are of the order of 40–50% of the amplitude of the lowest level after 24 hours. The difference

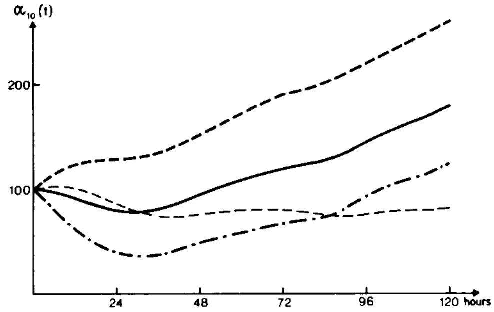

Fig. 7. Variation of the amplitude at 950 mb of a wave with a wavelength of 2000 km in both zonal and meridional directions. Full line shows the wave with no initial phase-lag, dashed line the wave with a negative initial phase-lag (tilting backwards) and the dash-dotted line the wave with a positive initial phase-lag (tilting forwards). Zonal wind, static stability and initial phase-lag are given in Table 2. Thin dashed line shows the wave which initially is tilted backwards but with Ekman friction included.

Table 2. *The zonal profile and the static stability used to study short baroclinic waves.* (a), (b) *and* (c) *give the initial phase for the three different experiments referred to in the text*

Pressure mb	v m/s	σ MTS-unit	Phase of the initial wave in degrees (a)	(b)	(c)
50	18	—	0	0	0
100	—	200			
150	33	—	0	0	0
200	—	30			
250	35	—	0	−2.5	+2.5
300	—	13			
350	26	—	0	−5	+5
400	—	4			
450	21	—	0	−7.5	+7.5
500	—	3			
550	16	—	0	−10	+10
600	—	2.8			
650	12	—	0	−15	+15
700	—	2.6			
750	−9	—	0	−20	+20
800	—	2.4			
850	5.5	—	0	−30	+30
900	—	2.2			
950	3	—	0	−45	+45
1000	—	2			

which is created during the first 24–30 hours is then kept during the rest of the integration. The phase speed of the wave at the lowest level is very little influenced by the initial tilt of the wave. After 24 hours the deviations are less than ±40 km which is less than 5% of the total distance the wave has moved during 24 hours.

A similar integration with a longer and a more unstable wave, $L = M = 4000$ km, is shown in Fig. 8. The phase-lags are identical to those given in

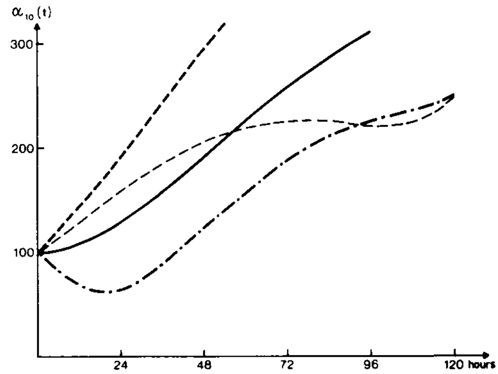

Fig. 8. The same as Fig. 7 but corresponding wavelengths are 4000 km.

Table 2 but in this case they will correspond to relatively larger errors namely ±500 km. Even in this case the deviations are of the order of 40–50% of the amplitude of the lowest level after 24 hours. As can be expected the effect on the phase speed is much larger in this case of a more unstable wave, and the fastest growing wave in (b) moves much slower than (a) and (c). The deviations are of the order of 500 km or 35% of the total distance the wave has moved during 24 hours. We have also included an integration with a different lower boundary condition incorporating the effect of an Ekman boundary layer. As can be seen from Fig. 5 and Fig. 6 incorporation of surface friction reduces the growth of the wave in particular for the shorter waves. However, during the first 24 hours the differences in the initial state create larger deviations.

We will next investigate the sensitivity of the equations (2.7) and (2.8) to errors in the initial state which may occur in reality. Over the major part of the globe we will have to rely on observing systems which generally will yield much larger analysis errors in the free atmosphere than at the surface.

The lack of observations as well as the existence of systematic errors in the satellite temperature soundings will give errors which in particular will reduce the amplitude of the geopotential fields in the free atmosphere (Bonner, 1976). Thus systematic error will most likely be reflected in all wave components including the ultra long waves. It has also been found that the amplitudes of ultra long waves are systematically underpredicted (Miyakoda et al., 1972 and Arpe et al., 1976). Since the forecast is used as a first guess this will imply systematically smaller amplitudes of the ultra long waves in the free atmosphere assuming an observing system currently being implemented. For the shorter waves we will also expect phase errors which also in general will increase by height. The nature of the phase error will depend on the assumption made about the vertical covariances applied in the objective analysis procedures. In most cases these imply a vertical structure given by the first guess.

Table 3. *The zonal profile and the static stability used to study baroclinic waves in the second experiment referred to in Section 4. Amplitude and phase "error" used in the experiment are also given*

Pressure mb	v m/s	σ MTS-unit	Amplitude error %	Phase error °
50	8.5	—	60	30
100	—	200		
150	27	—	60	30
200	—	30		
250	25	—	60	30
300	—	13		
350	23	—	55	28
400	—	4		
450	21	—	45	25
500	—	3		
550	19	—	40	21
600	—	28		
650	17	—	30	15
700	—	2.6		
750	15	—	15	8
800	—	2.4		
850	13	—	5	2
900	—	2.2		
950	11	—	0	0
1000	—	2		

Since our main interest for numerical prediction is to forecast the lower part of the atmosphere we will investigate to what extent errors in the phase and in the amplitude in the middle and upper part of the atmosphere will influence the wave in the lower part of the troposphere. We will investigate how this error varies within a function of the scale of wave. The assumed phase and amplitude errors are given in Table 3. In order to see the difference between stable and unstable waves more clearly we have reduced the baroclinicity of the zonal flow from that used in the preceding experiment (see Table 3). The profile given in Table 2 is not realistic to use for the very long waves. We have carried out the integration for 10 different scales of waves. Table 4 gives the percentage of the error due to error in the initial amplitude. The amplitude errors are rather small for short and medium size waves but become extremely large for the ultra long waves. At 36 hours the error of the amplitude has

Table 4. *The ratio in percentage between a wave with an initial error in the amplitude (see text) and the reference amplitude as a function of scale. The lowest two lines give the corresponding phase error in degrees as well as in kilometres after 36 hours*

Zonal wavelength Meridional wavelength km × 10^3	2 2	3 3	4 4	5 5	6 6	7 7	8 8	10 —	20 —
6 h	0.2	0.0	0.1	0.3	0.0	0.0	0.1	3.0	2.2
12 h	0.8	0.1	0.2	0.8	0.0	0.1	0.1	10.2	7.4
18 h	1.7	0.3	0.4	1.3	0.1	0.3	0.4	20.3	44.6
24 h	3.0	0.5	0.7	1.7	0.1	0.5	0.7	35.0	77.6
30 h	4.6	0.9	1.0	1.7	0.2	0.7	1.1	55.8	41.7
36 h	6.2	1.4	1.2	1.9	0.2	1.1	1.7	83.0	9.5
Phase error (in deg)	7.5	10.4	9.5	6.9	3.3	1.3	6.4	19.4	35.7
Phase error (in km)	42	87	106	96	55	25	142	539	1983

Table 5. *The ratio in percentage between a wave with an initial phase error (see text) and the reference atmosphere as a function of scale. The lowest two lines give the corresponding phase errors in degrees as well as in kilometres after 36 hours*

Zonal wavelength Meridional wavelength km × 10^3	2 2	3 3	4 4	5 5	6 6	7 7	8 8	10 —	20 —
6 h	2.1	2.5	2.2	1.9	0.6	0.4	0.2	13.6	29.1
12 h	4.3	5.1	4.4	4.2	1.3	0.8	1.0	28.4	25.6
18 h	6.2	7.6	6.7	6.4	2.0	1.1	2.1	40.5	9.7
24 h	7.8	9.9	8.8	8.6	2.6	1.5	3.5	43.7	29.9
30 h	9.4	12.2	10.8	10.5	3.2	1.7	4.7	30.4	22.0
36 h	10.3	14.4	12.6	12.5	4.0	2.0	6.1	2.5	5.1
Phase error (in deg)	2.3	0.3	1.4	1.1	0.1	1.3	8.1	8.3	0.5
Phase error (in km)	12	3	16	15	2	25	180	230	28

increased to 83% for $L = 10{,}000$ km. (A halving of the initial error yields a corresponding error at 36 h of 43%.) Also the phase error became substantial for the long waves. As we can see this is in agreement with the discussion in Section 3 (see eqs. 3.15 and 3.16).

In Table 5 we have in a similar way presented the result computed from error in the phase of the wave. This gives rise to large amplitude errors for the shorter waves and again in particular for the ultra long waves. The phase errors are in this case, where we have a flow which is only slightly baroclinically unstable, extremely small. Fig. 9 finally presents the variation of the amplitude at the lower level for a wave with a wavelength of 10,000 km.

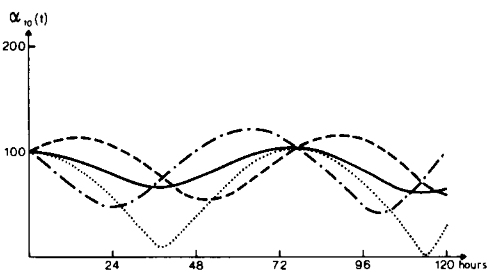

Fig. 9. Variation of the amplitude at 950 mb of a wave with a wavelength of 10,000 km in the zonal direction. Full line shows the wave with no initial phase-lag, dashed line the wave with a positive initial phase-lag (tilting forwards) and the dash-dotted line the wave with a negative initial phase-lag (tilting backwards). Zonal wind, static stability and initial phase-lag are given in Table 3. The dotted curve shows the effect of an assumed "amplitude" error in the middle and upper part of the atmosphere according to Table 3.

5. Conclusions

In the present study we have investigated the error growth for simple quasi-geostrophic models. It is found that the stable baroclinic waves in particular are sensitive to errors in the initial state. The structure at any given time for the stable waves is uniquely given by the initial conditions, whereas the structure of the unstable waves is given by the wind field and the stability field of the large scale flow. It is found that the initial specification of phase is very important and very small systematic error in the vertical tilt of the system yields an error growth which is much larger than significant physical processes such as friction in the boundary layer. Special care must be taken in specifying constraints on the vertical tilt of the weather systems in the objective analysis procedure.

6. Acknowledgements

The author wishes to express his thanks to the staff members of ECMWF for stimulating discussions throughout this work. He would very much like to thank Mrs. Jan Haseler for programming assistance and Mrs. Astrid Dinshawe for typing the manuscript.

7. Appendix

In order to carry out the integrations of (2.7) and (2.8) with high accuracy we have made an exact solution of eq. (2.8). Since we only have three diagonal elements in the corresponding matrix, we arrive at the following system

$$\begin{aligned}&\Omega_0 = 0\\ &\Omega_{k-1} - \lambda\Omega_k + \Omega_{k+1} = W_k \qquad (A.1)\\ &\Omega_N = F_N(k^2 + m^2)\psi_N\end{aligned}$$

We now introduce

$$\begin{aligned}&\alpha_0 = 0\\ &\omega_0 = 0\\ &\alpha_k = \frac{1}{\lambda - \alpha_{k-1}}\\ &\omega_k = \alpha_k(\omega_{k-1} - W_k) \qquad k = 1, \ldots N-1 \qquad (A.2)\\ &\Omega_N = F_N(k^2 + m^2)\psi_N\\ &\Omega_k = \omega_k + \alpha_k\Omega_{k+1} \qquad k \quad N-1, \ldots 1 \qquad (A.3)\end{aligned}$$

Equation (2.8) is integrated by a 4th order Runge-Kutta scheme. If we formally can write eq. (2.8) as

$$\frac{\partial\psi}{\partial t} = F(t)$$

we have the following procedure for 1 time-step.

$$\begin{aligned}\psi_*^{\tau+\frac{1}{2}} &= \psi^\tau + \frac{\Delta t}{2} F(\psi^\tau)\\ \psi_{**}^{\tau+\frac{1}{2}} &= \psi^\tau + \frac{\Delta t}{2} F(\psi_*^{\tau+\frac{1}{2}})\\ \psi_*^{\tau+1} &= \psi^\tau + \Delta t\, F(\psi_{**}^{\tau+\frac{1}{2}})\\ \psi^{\tau+1} &= \psi^\tau + \frac{\Delta t}{6}[F(\psi^\tau) + 2F(\psi_*^{\tau+\frac{1}{2}})\\ &\quad + 2F(\psi_{**}^{\tau+\frac{1}{2}}) + F(\psi_*^{\tau+1})] \qquad (A.4)\end{aligned}$$

(A.2)–(A.4) give a very accurate solution to eqs. (2.7) and (2.8). The relative numerical error is of around 10^{-5}.

REFERENCES

Arpe, K., Bengtsson, L., Hollingsworth, A. and Janjic, Z. 1976. A case study of a 10-day prediction. European Centre for Medium Range Weather Forecasts, Technical Report No. 1, 105 pp.

Bengtsson, L. 1964. Some numerical experiments on the effect of the variation of the static stability in two-layer quasi-geostrophic models. *Tellus 16*, 328–348.

Bengtsson, L. and Gustafsson, N. 1972. Assimilation of non-synoptic observations. *Tellus 24*, 383–399.

Bonner, W. D., Van Haaren, R. and Hayden, C. M. 1976. Operational-type analyses derived from satellite temperature soundings. NMC *Technical Report.*

Bretherton, F. P. 1966. Critical layer instability in baroclinic flows. *Q. J.R. Met. Soc. 92*, 325–334.

Brown, J. A., Jr. 1969. A numerical investigation of hydrodynamic instability and energy conversions in the quasi-geostrophic atmosphere. Part I. *J. Atmos. Sci. 26*, 352–365.

Gandin, L. S. 1960. *Objective analysis of meteorological fields.* Gidrometeorologicheskoe, Izdatelstro, Leningrad 1960. Translated from Russian into English, Israel Program for Scientific Translations, Jerusalem 1965.

Green, J. S. A. 1960. A problem in baroclinic stability. *Q. J.R. Met. Soc. 86*, 237–251.

Hirota, I. 1968. On the dynamics of long and ultra long waves in a baroclinic zonal current. *J. Met. Soc. Japan 46*, 234–249.

Miyakoda, K., Hembree, G. D., Strickler, R. F. and Shulman, J. 1972. Cumulative results of extended forecast experiments. I. Model performance for winter cases. *Mon. Weather Rev. 100*, 836–855.

Moen, L. 1974. A spectral model for investigation of amplifying baroclinic waves. *Tellus 26*, 424–443.

Ogura, Y. 1957. Wave solutions of the vorticity equation for the 2½-dimensional model. *J. Meteorol. 14*, 60–64.

Robert, A. 1974. GARP activities related to computational considerations. GARP Working Group on Numerical Experimentation, Progress Report No. 4, 2–23.

СКОРОСТЬ РОСТА И ВЕРТИКАЛЬНОЕ РАСПРОСТРАНЕНИЕ НАЧАЛЬНОЙ ОШИБКИ В БАРОКЛИННЫХ МОДЕЛЯХ

В настоящей работе исследуется скорость роста ошибки при расчетах бароклинных волн. Найдено, что устойчивые или нейтральные волны особенно чувствительны к ошибкам в начальных условиях. Короткие устойчивые волны чувствительны в основном к ошибкам фазы, в то время как ультрадлинные волны чувствительны к ошибкам амплитуды. Эксперименты по моделированию анализа показывают, что амплитуды очень длинных волн обычно очень малы в свободной атмосфере из-за редкого и крайне нерегулярного распределения наблюдений в свободной атмосфере. Это же относится и к экспериментам по четырехмерному усвоению данных, так как амплитуды очень длинных волн обычно получаются заниженными. Численные эксперименты, приводимые здесь, показывают, что если очень длинные волны содержат ошибки в амплитуде указанного типа в верхней тропосфере или нижней стратосфере, то ошибка быстро распространяется (в течение суток или двух) до нижней тропосферы и до поверхности.